

Nondestructive Dimension Sorting by Soft Robotic Grippers Integrated with Triboelectric Sensor

Sheng Zhang,¹ Baosen Zhang,¹ Da Zhao, Qi Gao, Zhong Lin Wang,^{*} and Tinghai Cheng^{*}

Cite This: <https://doi.org/10.1021/acsnano.1c10396>

Read Online

ACCESS |

Metrics & More

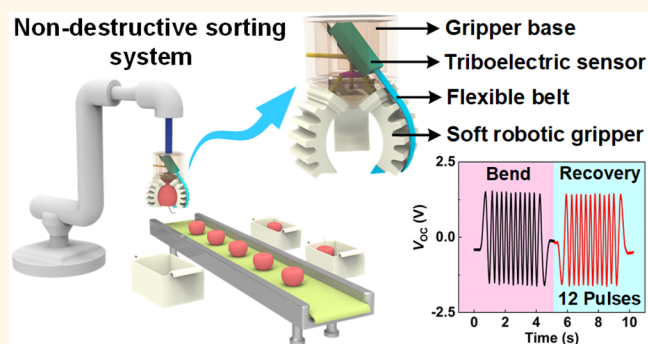
Article Recommendations

Supporting Information

ABSTRACT: In smart logistics, traditional manual sorting and sorting systems based on rigid manipulators limit the warehousing development and damage the goods. Here, a non-destructive sorting method based on bionic soft fingers is proposed. This method is implemented by the soft robotic gripper (SRG) for grasping of the breakable objects, the triboelectric sensor (TES) for size sorting of the objects, and the signal processing module. In the fabrication of SRG, the silicon rubber is prepared by controlling the material synthesis process, and its Young's modulus is 600.91 kPa, which is comparable to the Young's modulus of skin tissue. Also, the maximum input pressure of SRG is 71.4 kPa. The TES has a linear relationship between pulse number and sliding displacement, and its resolution is 3 mm. It induces pulse signal sequences to quantify the SRG bending state and thus realize the size sorting of objects. Additionally, a nondestructive sorting system based on TES and SRG has been developed for fruit sorting (e.g., apples, oranges), enabling nondestructive grasping and accurate sorting. Its sorting range is 70–120 mm, and the sorting accuracy rate is up to 95%. This work also provides a way for the application of SRG and triboelectric sensors in the sorting field.

KEYWORDS: smart logistics, warehousing management, nondestructive sorting, soft robotic gripper, triboelectric sensor

Smart systems based on the Internet of Things (IoT), such as smart medical care, smart home furnishings, and smart cities, have achieved vigorous development, thus promoting the rapid development of the social economy.^{1–4} In 2009, a concept, smart logistics, was introduced in China. Smart logistics refers to the modern logistics mode that realizes intelligent analysis and improves the logistics operation efficiency through cyber-physical systems, IoT, and other intelligent technical means.^{5,6} In the smart logistics system, the warehousing pays an irreplaceable role in fulfilling logistics orders. Currently, the traditional manual operation leads to warehousing management efficiency and is no longer responsive to the logistics requirements.⁷ Among the management in all the warehousing, research studies found that the goods sorting process is the major bottleneck of the warehousing development and accounts for 50–55% of total operating expenses.⁸ To make up for the shortcomings of manual sorting flexibility and limited operation efficiency, the rigid manipulator has made great progress in the goods sorting system.⁹ In recent years, with the dimension of objects as the sorting basis, the rigid manipulators are designed and assembled into a three-gripper mode for the



sorting of spherical objects. The frequently used sorting sensors are mostly machine vision and infrared sensing, etc.^{10,11} Nevertheless, the rigid manipulator is mostly made of metal materials, resulting in poor safety, limited adaptability, and insufficient flexibility. Especially in fruit warehousing management, it is easy to cause epidermis damage and difficult to achieve nondestructive sorting, thus resulting in the pecuniary loss of fruit. Meanwhile, it is complicated and expensive to rely on sensing technologies such as machine vision and infrared sensing. As consequence, the sorting system based on a rigid manipulator is not conducive to generalized application in fruit warehousing management.

Received: November 23, 2021

Accepted: February 3, 2022

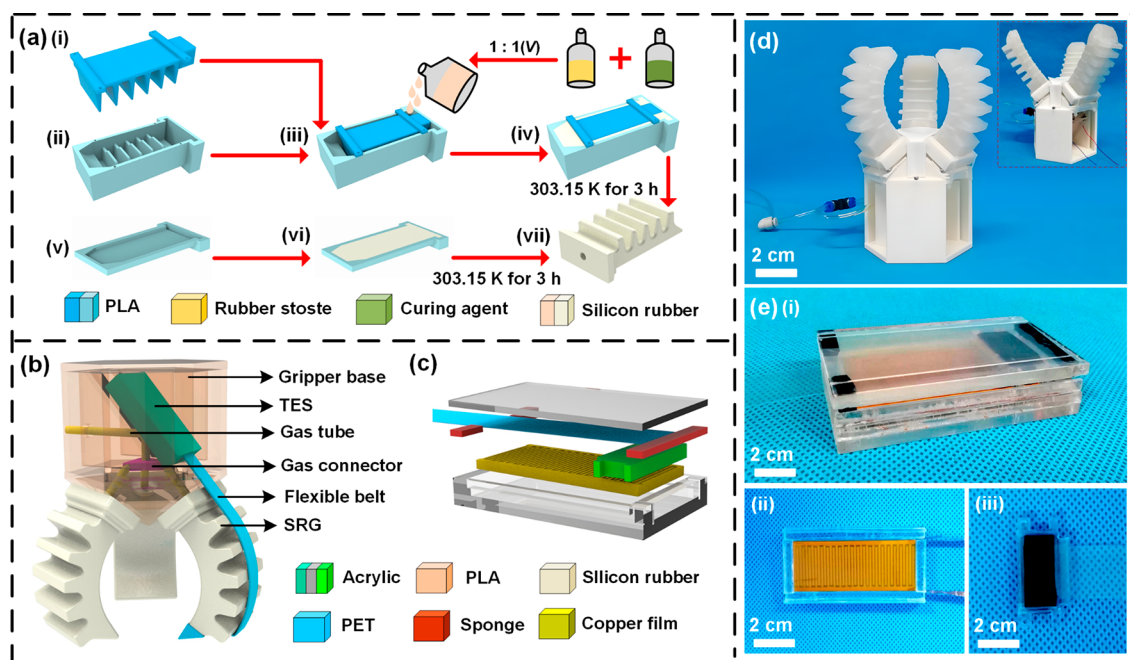


Figure 1. Structural design and fabrication of the TS-SRG: (a) flow-process diagram of the SRG, (b) schematic structure of the TS-SRG, (c) schematic structure of the TES, (d) photographs of the TS-SRG prototype, and (e) photographs of the TES prototype.

In nature, organisms are flexible through soft tissues and can quickly adapt to complex environments. Based on bionic thought, researchers use soft materials, such as polymers, intelligent materials, and multifunctional materials, to make soft robotics to realize safe and efficient interaction with the environment.^{12,13} With the objects size as the sorting basis, the sorting system designed with the soft robotic gripper (SRG) is expected to realize nondestructive grasping in spherical fruits sorting.¹⁴ Also, classification by fruit size is beneficial to better reflect the economic value of fruit itself. Nonetheless, at present, the SRG lack matching sorting sensors to form a sorting system to realize fruits sorting management. A triboelectric nanogenerator (TENG, also called as Wang generator) was proposed by Wang's group in 2012.¹⁵ It can convert mechanical stimulations into electrical signals by the coupling effect of contact electrification and electrostatic induction.^{16,17} In recent years, the rapid development of the TENG provides a possibility for the SRG to be used for fruits sorting management.^{18–20} TENG has the advantages of low cost,²¹ multiple working mode,²² diverse structure,^{23,24} and high voltage,²⁵ which can be used as both energy collection device and distributed sensors. Also, TENG, as an active sensor, can collect energy from the surrounding environment and acquire self-powered ability without external power supply.²⁶ Currently, the amplitude of the pulse signals is usually used as the output parameter of triboelectric sensor performance.^{27–29} Whereas, the performance output of the sensor based on this mode is not always accurate in some applications, as there are so many factors influencing the amplitude, such as temperature,³⁰ humidity,³¹ and human-made interference,³² which will be different in each measurement result. Based on the above problem, using the pulse number as the output parameter of the sensor will be a robust and reliable sensing mechanism.

Herein, a nondestructive sorting method based on bionic soft fingers is proposed. This method is implemented by the SRG for grasping of breakable objects, the triboelectric sensor (TES) for size sorting of objects, and the signal processing module. In

fabrication of the SRG, the silicon rubber is controlled by adjusting the material synthesis process. Meanwhile, its tensile resistance and Young's modulus have also been investigated. Based on the sensitivity of TENG to mechanical motion, the TES with a grating-like electrode induces a pulse signal sequence using the sliding motion of the slider relative to the electrode to realize the quantification of the SRG bending deformation state. Also, a mathematical model between the diameter of SRG and pulse number is established and proven to be feasible. Additionally, a nondestructive sorting system based on TES and SRG (TS-SRG) has been developed for fruit sorting (e.g., apples, oranges), enabling nondestructive grasping and accurate sorting. This work also provides a way for the application of SRG and TENG in the sorting field.

RESULTS AND DISCUSSION

Structural Design and Materials Option. A soft printing process combined with mold design is used for the fabrication of SRG, with the specific process as shown in Figure 1a. The silicon rubber liquid is prepared by controlling the volume ratio of the rubber stoste and curing agent after uniform mixing. The silicon rubber liquid is poured into predesigned and processed SRG molds. Subsequently, the poured SRG molds are placed in a heated environment for the cross-linking reaction. Finally, the SRG is obtained by removal of the mold and treatment after the reaction and cooling to room temperature. The SRG mold printed by three-dimensional (3D) print technique and the SRG poured by silicon rubber are given in Figure S1a,b, respectively. The schematic structure of the TS-SRG is illustrated in Figure 1b. It consists of a flexible belt, three SRGs, a gas connector, four gas tubes, a TES, and a polylactic acid (PLA) gripper base. The SRG as a terminal device is used to complete the grasping of the spherical objects. The flexible belt acts as a connection between the SRG and the TES to transmit the bending deformation of the SRG, so that the TES can complete the pulse signal output. The gas source provides power for the bending deformation of the SRG. The schematic structure of the TES with grating-like

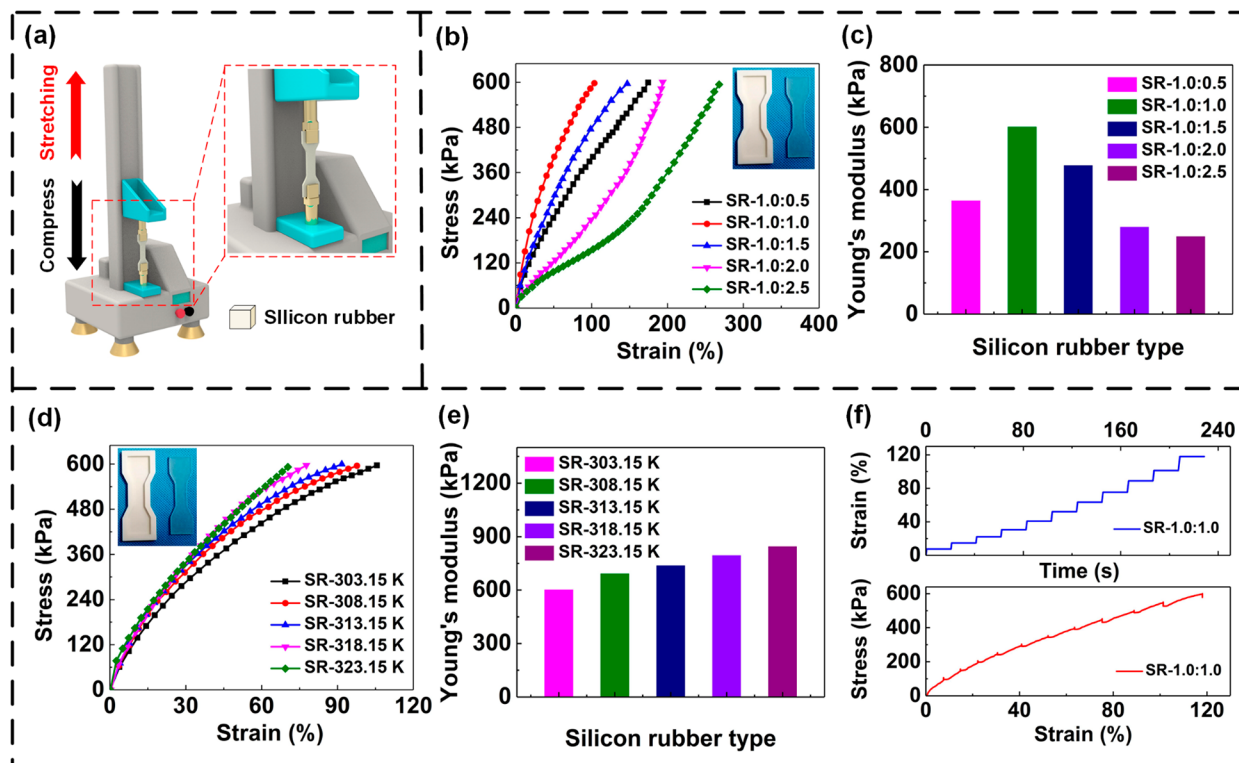


Figure 2. Preparation and tensile properties of the silicon rubber: (a) Stretching schematic diagram of the silicon rubber, (b) tensile properties, and (c) Young's modulus of the silicon rubber at different volume ratios; (d) tensile properties and (e) Young's modulus of the silicon rubber at different reaction temperatures; (f) step stretching of the silicon rubber.

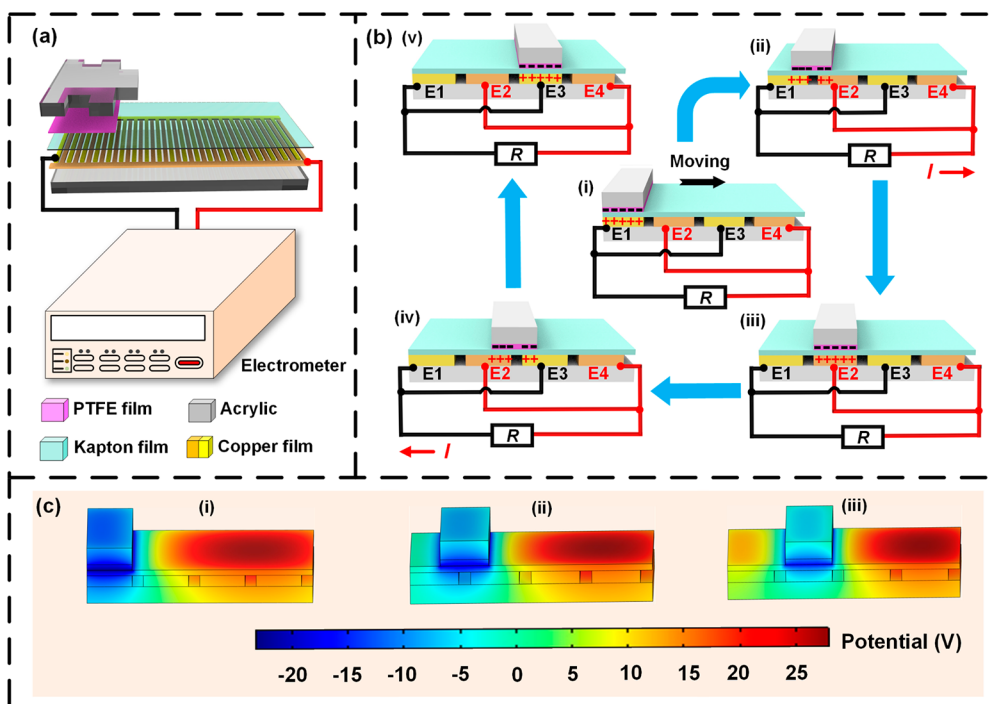


Figure 3. Operating principle and simulation of the TES: (a) Schematics of the grating-like electrode part and the slider part, (b) schematics of the electron transfer process in the sliding, and (c) simulations of the device in three states.

electrode is shown in Figure 1c. Figure 1d shows a photograph of the assembled TS-SRG. The photograph of the TES is given in Figure 1e(i). The TES is divided into two main parts: the grating-interdigitated electrode [Figure 1e(ii)] and the slider [Figure 1e(iii)]. This electrode consists of a layer of Kapton film,

a flexible printed circuit board, and an acrylic board base. This slider consists of a polytetrafluoroethylene (PTFE) film, a black sponge glue, and an acrylic board base.

In the fabrication of SRG, the selection and preparation of soft materials are particularly important for a large deformation state.

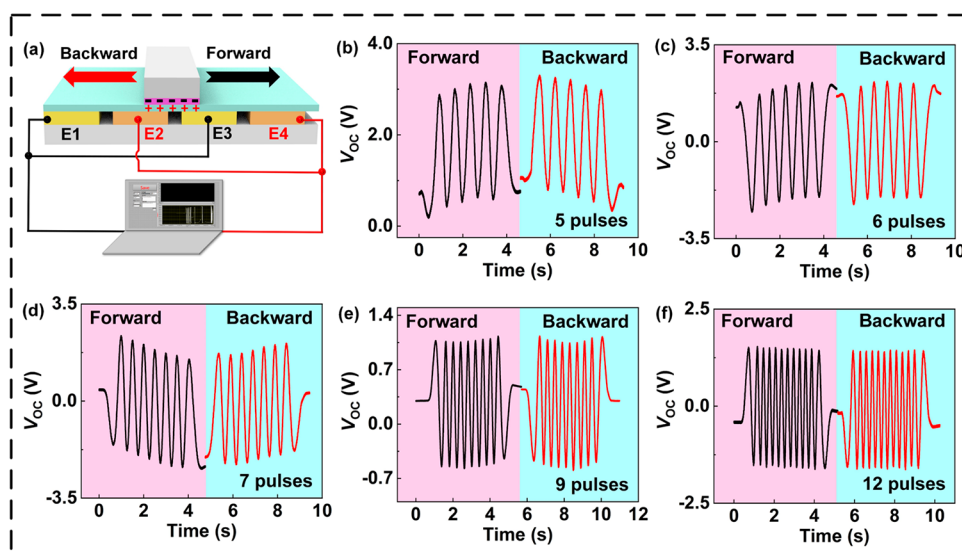


Figure 4. Open-circuit voltage output characteristics of the TES under different grating spacing: (a) The sliding schematics of the grating-like electrode part and the slider part and (b–f) pulses generated by the TES with different grating spacings ($d_1 = 2.5$ mm, $d_2 = 2.0$ mm, $d_3 = 1.5$ mm, $d_4 = 1.0$ mm, $d_5 = 0.5$ mm) under the same sliding displacement ($\Delta L = 36$ mm) and sliding speed ($v = 10$ mm/s).

Consequently, the silicon rubber is controlled by adjusting the different volume ratios of rubber stoste and curing agent and the different reacting temperatures. The prefabricated silicon rubber liquid is poured into a stretching mold to obtain a silicon rubber sheet to investigate its tensile properties and Young's modulus. A stretching diagram of the silicon rubber sheet is shown in Figure 2a. In the reacting temperature at 303.15 K, the effects of the volume ratio of rubber stoste and curing agent at 1.0:0.5, 1.0:1.0, 1.0:1.5, 1.0:2.0, and 1.0:2.5 on tensile properties and Young's modulus are investigated and shown in Figure 2b,c, respectively. Under the same stretching stress, the SR-1.0:1.0 exhibits excellent tensile strength compared to the others, and its Young's modulus is 600.91 kPa, which is comparable to the Young's modulus of the skin tissue^{33,34} and satisfies the needs of SRG bending deformation. Moreover, in the volume ratio at 1.0:1.0, the effects of reacting temperature at 303.15, 308.15, 313.15, 318.15, and 323.15 K on tensile properties and Young's modulus are investigated and shown in Figure 2d,e. As a result, the tensile strength and Young's modulus of silicon rubber increase with the increase in reacting temperature. The step stretching of SR-1.0:1.0 was explored in Figure 2f, and its stretching strain increases with the increase of stretching stress. It is necessary to evaluate the durability and load/unload cycle performance test of silicon rubber. The durability and load/unload cycle performance of SR-1.0:1.0 are tested using the tensile method at the test speed of 20 mm/min and test distance of 16 mm. In the durability test, the SR-1.0:1.0 are loaded and unloaded for 5.5 h at the same strain and stress, respectively, as shown in Figure S3b. In the load/unload cycle performance test, the SR-1.0:1.0 is loaded and unloaded for 500 cycles in Figure S3c. There are obvious hysteresis loops in the loading and unloading process. With the increase of loading and unloading times, the overall stress–strain curves tend to shift to the right and the offset is smaller than the previous one, and a stable and closed hysteresis loop is formed at last.

Operational Principle and Simulation. The mechanical energy in the TES comes from the relative sliding of the grating-like electrode and the slider caused by the bending deformation of the soft grippers, so the deformation state of the soft finger can

receive feedback from the pulse electrical signal generated by the TES. As shown in Figure 3a, the grating-like electrode and the slider form a relative sliding freestanding mode. The operating mechanism of the TES is illustrated in Figure 3b. The slider is wholly aligned with the E1 of the grating-interdigitated electrode [Figure 3b(i)]. As the slider is pasted on the Kapton film, the positive charges of E1 are equal to the negative charges on the surface of the PTFE. There is no charge transfer between electrode E1-E3 and E2-E4 due to electrostatic equilibrium. When the slider is sliding relative to the grating-interdigitated electrode, the E2-E4 will generate positive charges under the action of the triboelectric effect [Figure 3b(ii)], which will cause electrons to flow between the E1-E3 and E2-E4 to form a new electrostatic equilibrium, causing the external load to form a transient current. Once the slider completely overlaps the E2 [Figure 3b(iii)], all the electrons are transferred to the electrode E1, and the electrostatic equilibrium between the slider and E2 is reached again. Similarly, as the slider slides, electrons return from electrode E1-E3 to electrode E2-E4 [Figure 3b(iv)] until they coincide with the E3 [Figure 3b(v)]. Consequently, an alternating current signal is generated during the entire relative sliding period. To elucidate the working principle, the potential distribution of the grating-like electrode part and the slider part is simulated by COMSOL Multiphysics 5.6 under an open-circuit state, as shown in Figure 3c. The potential contour clearly shows that Kapton is in different contact positions with PTFE, resulting in a potential difference between the two electrodes that drives the flow of charge in the external circuit. The electrostatic potential simulation conditions and parameters are presented in the Supporting Information (Note S1).

Output Characteristics. The schematic diagram of the forward/backward sliding induced by reciprocating horizontal movement of the stepping motor is shown in Figure 4a. To improve the sensing accuracy, the TESs with different grating spacings ($d_1 = 2.5$ mm, $d_2 = 2.0$ mm, $d_3 = 1.5$ mm, $d_4 = 1.0$ mm, and $d_5 = 0.5$ mm) are manufactured for studying the sensing accuracy. The flexible belt of TES is controlled to be stretched or released by the stepping motor under the same sliding displacement ($\Delta L = 36$ mm) and sliding speed ($v = 10$ mm/

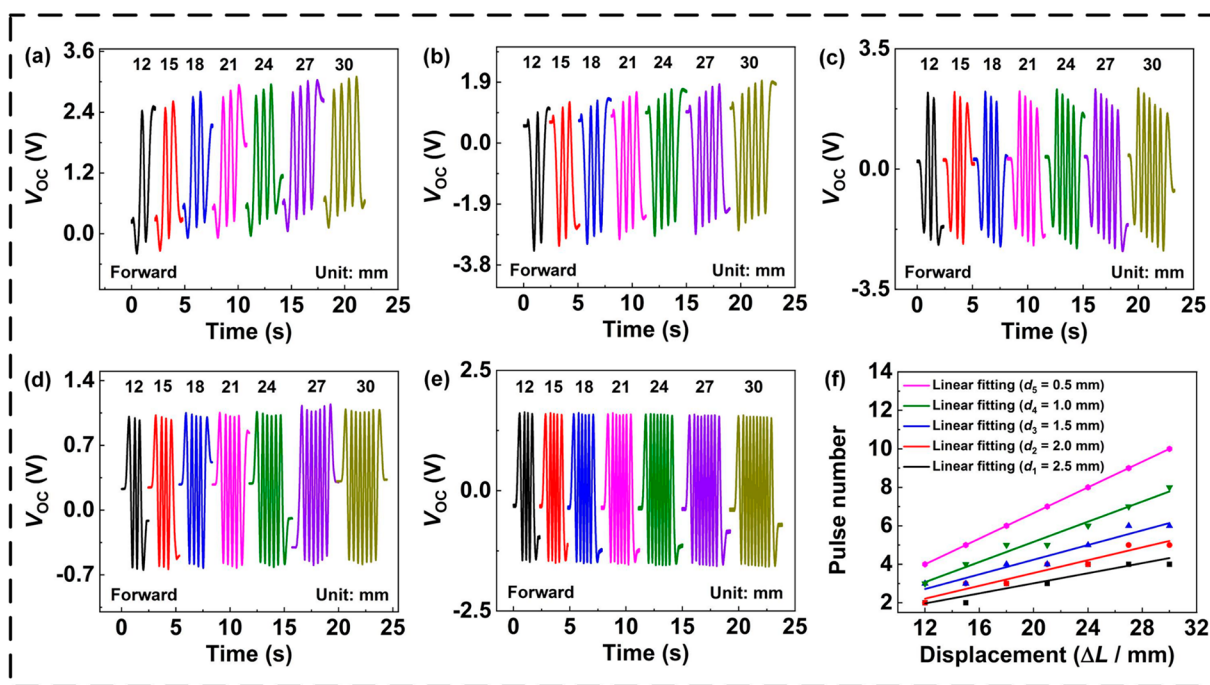


Figure 5. Open-circuit voltage output characteristics of the TES under different sliding displacements: (a–e) The pulses generated by the TES with grating spacing ($d_1 = 2.5$ mm, $d_2 = 2.0$ mm, $d_3 = 1.5$ mm, $d_4 = 1.0$ mm, $d_5 = 0.5$ mm) when the sensor has different sliding displacement at the same sliding speed ($v = 10$ mm/s); (f) the linear relationship between the sliding displacement and the number of the pulses generated by the TES.

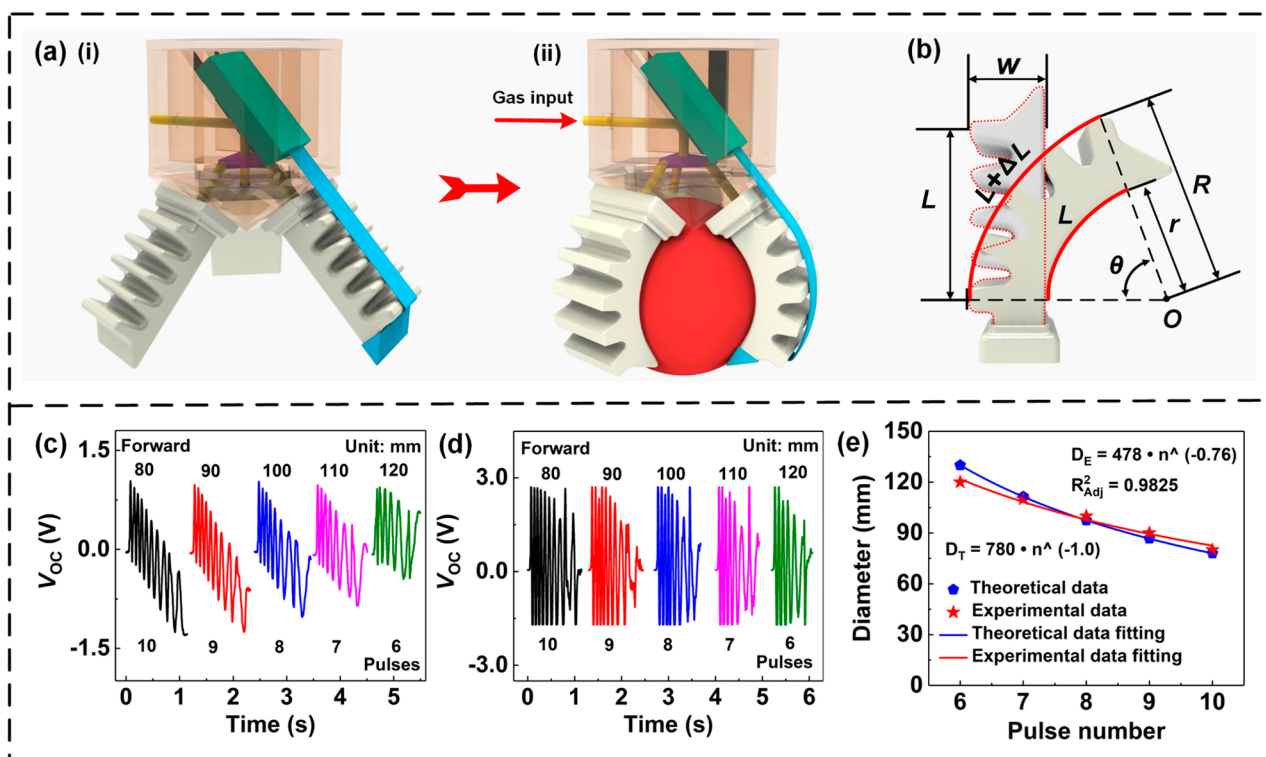


Figure 6. Sensing characteristics of the TS-SRG: (a) Schematics of the operation mechanism of the TS-SRG, (b) the dimension measuring principle of the TS-SRG; (c) the pulse output characteristics of the TS-SRG with load test objects of different diameter, (d) the pulse output characteristics of the TS-SRG after signal processing, (e) the diameter and pulse number fitting curves.

s), and the signals generated during the stretching process (marked as forward) and releasing process (marked as backward) can be seen in Figure 4b–f. The pulse numbers of the TES are 5, 6, 7, 9, and 12 at grating spacings of 2.5 mm, 2.0

mm, 1.5 mm, 1.0 mm, and 0.5 mm, respectively. These findings suggest that finer grating gaps induce more pulses under the same sliding displacement and sliding speed, which will bring better accuracy for the application of size measurement.

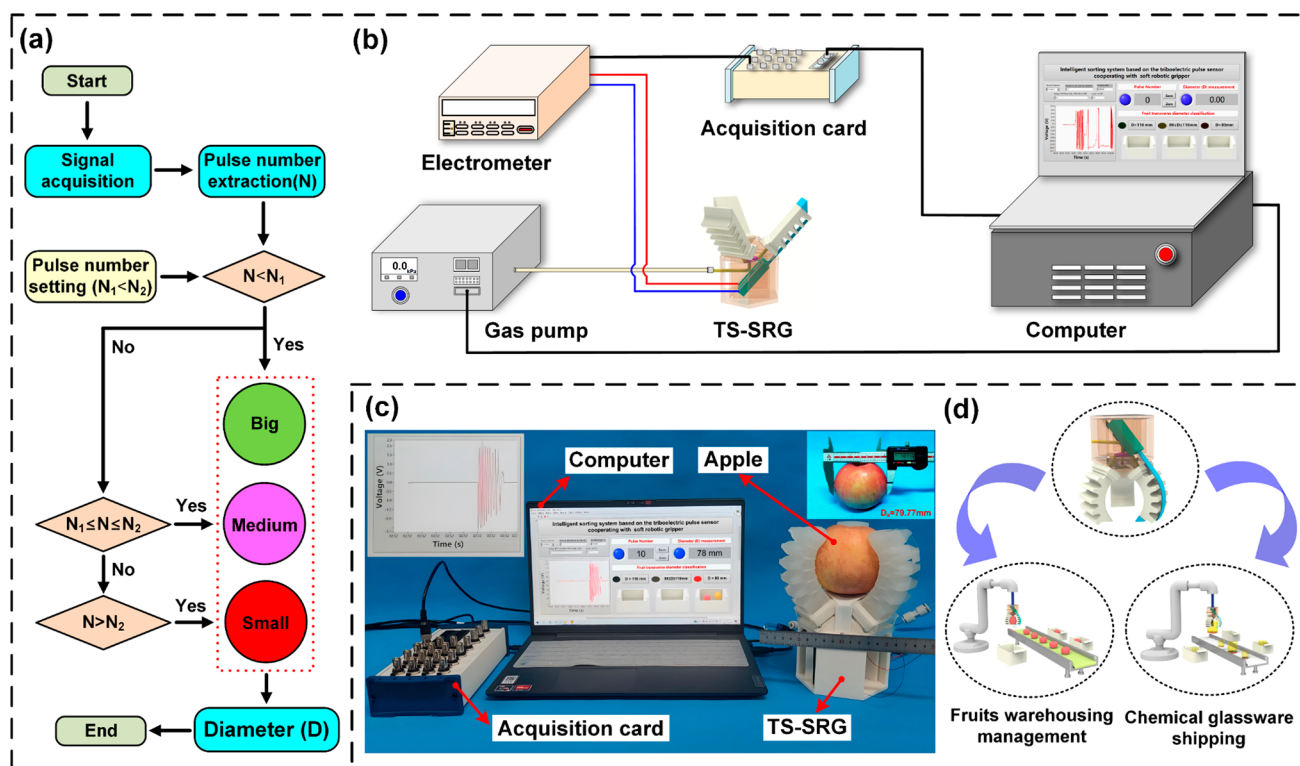


Figure 7. Application and demonstration of the nondestructive sorting system based on the TS-SRG in practical applications: (a) The program chart of nondestructive sorting system; (b) the block diagram of the output system of the TS-SRG; (c) the practical demonstration of the TS-SRG for fruit sorting application; (d) the diagram of the TS-SRG application prospect.

Moreover, the pulse number of forward motion for the TES is the same as that of the backward motion, which can also reflect that it has a stable pulse signal output to a certain extent. More short-circuit current and transferred charge pulse details of TES with different grating spacing can be shown to Figures S4 and S5, respectively.

In order to research the relationship between the slider displacement and pulse number, the TES is driven by the stepper motor at 10 mm/s to generate different sliding displacements ($\Delta L = 12$ mm, 15 mm, 18 mm, 21 mm, 24 mm, 27 mm, and 30 mm), and then the corresponding pulse sequences are recorded, respectively, as illustrated in Figure 5a–e. More data are referred to Table S2. The short-circuit current and transferred charge pulse details of TES are shown in Figures S6 and S7, respectively. The figures show that the pulse number of each sequence of pulses is linear to the sliding displacement (Figure 5f), and also, the fitting lines between pulse number and displacement of the TES with different grating spacing have different slopes ($S_{d1} = 0.13$, $S_{d2} = 0.17$, $S_{d3} = 0.19$, $S_{d4} = 0.26$, $S_{d5} = 0.33$, definition: S represents the slope), which define these slopes as the displacement resolution. The finer grating gap segment will bring higher pulse numbers and a larger slope to the TES, that is, higher displacement resolution. Moreover, to explore the effect of the speed on the pulse number, the TES ($d_s = 0.5$ mm) is driven by the stepping motor to slide through 24 mm at different sliding speeds ($v = 3$ mm/s, 5 mm/s, 10 mm/s, 15 mm/s, and 20 mm/s). From Figure S8, the pulse width changes with the rotation speed, but the total pulse number is equal, which means that the TES can be robustly used for displacement sensing. It is necessary to evaluate the stable output of the pulse signal for the TES. The TES is operated continuously for 10 h with a sliding displacement of 30 mm (Figure S9a), and then the

corresponding pulse sequences at different moments are recorded, respectively, as illustrated in Figure S9b. The experimental results show that the TES can ensure the stable and accurate output of pulse signals after 10 h of continuous operation.

To investigate the grasping characteristics of the TS-SRG, the SRG was powered by pneumatic equipment. The left surface of the SRG is formed in a corrugated structure with low hardness and higher tensile ability. Meanwhile, the right surface is the same material without corrugated structure, which is relatively harder to deform. Thus, the SRG is driven by the pressure difference between the chamber and the external environment to cause bending, and the left surface tends to undergo larger deformation, as shown in Figure 6a. This bending deformation was transmitted through the flexible belt to the TES, to lead a sliding displacement of the slider part relative to the grating electrode part, thereby producing pulse signals. Whereas, it is necessary to evaluate the bending degree variations at the same input air pressure for the soft gripper with TES or not, that is, it must be confirmed that the load TES does not cause changes in the workspace or mechanical properties of the soft gripper. The test results indicated that the load TES has hardly any effect on the bending state of the soft gripper at different input air pressures, as shown in Figure S10. According to related previous works,^{18,35} the deformation of the SRG can be considered as an arc of a circle, and L and W are constant values. Based on the motion state of TS-SRG, a mathematical model of the arc length variation quantity (ΔL) and radius (r) after SRG bending can be established in Figure 6b and referred to in Note S2 of the Supporting Information. The state of TS-SRG grasping objects with different diameters is shown in Figure S11. Experimental results show that the pulse numbers of the TS-SRG are 10, 9, 8,

7, and 6 at corresponding diameters of 80, 90, 100, 110, and 120 mm in Figure 6c, respectively. The measured pulse signals have the following main problems: First, the baseline offset origin of the waveform, and second, the signal shows an upward trend. These problems may be due to an unstable air pressure input. To obtain regular signals and ensure the accuracy of signal acquisition, the original signal needs to be preprocessed by an amplifier. The measured results are shown in Figure 6d, which are consistent with the Figure 6c. The experimental data of the pulse number and the corresponding diameter fitting curve (marked in red) are shown in Figure 6e.

Demonstration. In smart logistics, traditional manual sorting and sorting systems based on rigid manipulators significantly limit the development of fruit warehousing and bring the pecuniary losses of the fruits. The program of the nondestructive sorting system is given in Figure 7a. The nondestructive sorting system includes the drive module, the TS-SRG module, the amplifier module, the acquisition card module, and the display module. First, the output signal is generated from the TS-SRG when the SRG is driven by the gas pump. Next, the output signal is processed through the amplifier before entering the NI acquisition card to obtain regular signals and ensure the accuracy of signal acquisition using the NI acquisition card. The amplified output signals are collected by the NI acquisition card, and the signals are counted by the LabVIEW software as the basis of fruit sorting. Finally, the count results are sent to the computer and displayed, as depicted in Figure 7b. Moreover, to verify the practical application of this system, the spherical fruits (e.g., apples and oranges) of different diameter (D) and species were grasped by the TS-SRG for fruit sorting, as shown in Figure 7c. There are three sorting grades: big ($D > 110$ mm), medium ($80 \text{ mm} \leq D \leq 110$ mm), and small ($D < 80$ mm). The error rate of measurement is only 2.22%, and sorting range is 70 mm to 120 mm. The detailed demonstration process is given in Video S1. To better illustrate the accuracy of this sorting system, the apples with different diameters ($D_a = 108.66$ mm, $D_a = 101.09$ mm, $D_a = 79.77$ mm) are repeatedly grasped 100 times, respectively. The test results are shown in Figure S12a. The sorting accuracy rates are 92%, 95%, and 93%, respectively. The reason for this test result may be attributed to the irregularity of the apple shape, the instability of the SRG driven by gas pump, and the grating width and spacing of the TES. Moreover, in Figure S12b, we have added the comparison in the recognition accuracy with other literatures.^{18,36–39} In a future application scenario, the TS-SRG can be combined with a robotic arm to perform fruit warehousing management and chemical glassware shipping, etc., as shown in Figure 7d. This work provides a research way for the practical application of the TENG in the sorting field.

CONCLUSIONS

In summary, a nondestructive sorting method based on bionic soft fingers is proposed. This method is implemented by the soft robotic gripper (SRG) for the grasping of breakable objects, the triboelectric sensor (TES) for size sorting of the objects, and the signal processing module. In the fabrication of SRG, the silicon rubber is prepared by controlling the material synthesis process, and its Young's modulus is 600.91 kPa, which is comparable to the Young's modulus of skin tissue. Also, the maximum input pressure of SRG is 71.4 kPa. The TES with grating-like electrode has a linear relationship between pulse number and sliding displacement, and its minimum displacement resolution is 3 mm. It induces a pulse signal sequence to realize the

quantification of the SRG bending state. Moreover, a non-destructive sorting system based on TES and SRG (TS-SRG) has been developed for fruit sorting (e.g., apples, oranges), enabling nondestructive grasping, size measurement, and accurate sorting. The error rate of measurement is only 2.22%, sorting range is 70 to 120 mm, and sorting accuracy rate is up to 95%. This work also provides a way for the application of SRG and TENG in the sorting field.

EXPERIMENTAL SECTION

Fabrication of the SRG. The fabrication of SRG was acquired using a soft printing process combined with mold design. The silicon rubber is prepared by controlling the different volume ratios of rubber stoste and curing agent and the different reaction temperatures after uniform mixing. The specific experimental parameters of volume ratio and reaction temperature are shown in Table S1. In the fabrication of SRG, the silicon rubber liquid with a volume ratio of 1.0:1.0 is poured into predesigned and processed SRG molds under the drainage of a drainage glass rod. The polylactic acid (PLA) molds of SRG are shown in Figure S1a. Subsequently, the poured SRG mold was kept at a temperature of 303.15 K for 3 h. Finally, the SRG was obtained by removal of the mold and treatment after the reaction and cooling to room temperature, as shown in Figure S1b.

Fabrication of the TES. The process of TES can be divided into the manufacturing of electrode and slider part and the assembling of the device. The TES consists of an acrylic box, an electrode part, and a sliding part. The acrylic board of 3 mm was cut and glued into the box. For the electrode part, an acrylic board was cut as the base board, as shown in Figure S2a. Then, the copper electrode with grating-like pattern was covered with the surface of the base board. This grating-like electrode is made from copper (thickness: 35 μm), which was processed using printed circuit board technology. Later, Kapton film was covered with the surface of grating-like copper electrode as the triboelectric positive electric layer. For the sliding part, an acrylic sheet was cut as the slider [Figure S2b]. The black sponge (thickness: 1.5 mm) is pasted to the slider surface for better contact with the electrode portion. Then, the PTFE serves as a triboelectric negative electric layer on a slider with black sponge, and the slider part is connected to flexible belt. Lastly, the slider, the electrode part, and the acrylic box are assembled into the TES.

Fabrication of the TS-SRG. The TS-SRG is composed of three SRGs, a flexible belt, a TES, a gas source, and a PLA gripper base. The PLA gripper base was printed by a 3D printer. The SRG was adopted to realize the grasping of the object. The flexible belt acted as a connection between the SRG and the TES to transmit the bending deformation of the soft gripper so that the TES can complete the pulse signal output. The gas source provided power for the bending deformation of SRG.

Electrical Measurement. The flexible belt of TES is driven by the stepping motor (57BYGH56D8EIS-P, HOHI, China) to control the slider. A software platform was constructed based on LabVIEW software and data acquisition card (BNC-2120, National Instruments, USA) for data acquisition and analysis. An electrometer (6514, Keithley, USA) was adopted to measure the open-circuit voltage, short-circuit current, and transferred charge signal. An amplifier (AD620, China) was used to amplify the electrical signal.

ASSOCIATED CONTENT

Supporting Information

The Supporting Information is available free of charge at <https://pubs.acs.org/doi/10.1021/acsnano.1c10396>.

Preparation of the SRG; fabrication process of TES; the durability and load/unload cycle performance test of silicon rubber; short-circuit current output characteristics of the TES under different grating spacing; transferred charge output characteristics of the TES under different grating spacing; short-circuit current output characteristics of the TES under different sliding displacement;

transferred charge output characteristics of the TES under different sliding displacement; pulse output characteristics of the TES under different sliding speed; the stability of the pulse signal output of TES after 10 h of continuous operation; bending test of the SRG in different input gas pressure; photograph of the TS-SRG for grasping spherical objects; sorting accuracy of the TS-SRG (PDF)

Video S1: Nondestructive sorting system based on triboelectric pulse sensor cooperating with soft robotic gripper (MP4)

AUTHOR INFORMATION

Corresponding Authors

Zhong Lin Wang – Beijing Institute of Nanoenergy and Nanosystems, Chinese Academy of Sciences, Beijing 101400, China; School of Nanoscience and Technology, University of Chinese Academy of Sciences, Beijing 100049, China; CUSTech Institute of Technology, Wenzhou, Zhejiang 325024, China; School of Materials Science and Engineering, Georgia Institute of Technology, Atlanta, Georgia 30332-0245, United States; orcid.org/0000-0002-5530-0380; Email: zhong.wang@mse.gatech.edu

Tinghai Cheng – Beijing Institute of Nanoenergy and Nanosystems, Chinese Academy of Sciences, Beijing 101400, China; School of Nanoscience and Technology, University of Chinese Academy of Sciences, Beijing 100049, China; CUSTech Institute of Technology, Wenzhou, Zhejiang 325024, China; orcid.org/0000-0003-0335-7614; Email: chengtinghai@binn.cas.cn

Authors

Sheng Zhang – Beijing Institute of Nanoenergy and Nanosystems, Chinese Academy of Sciences, Beijing 101400, China; School of Nanoscience and Technology, University of Chinese Academy of Sciences, Beijing 100049, China

Baosen Zhang – Beijing Institute of Nanoenergy and Nanosystems, Chinese Academy of Sciences, Beijing 101400, China; School of Nanoscience and Technology, University of Chinese Academy of Sciences, Beijing 100049, China; orcid.org/0000-0003-1747-8636

Da Zhao – Beijing Institute of Nanoenergy and Nanosystems, Chinese Academy of Sciences, Beijing 101400, China

Qi Gao – Beijing Institute of Nanoenergy and Nanosystems, Chinese Academy of Sciences, Beijing 101400, China; School of Nanoscience and Technology, University of Chinese Academy of Sciences, Beijing 100049, China

Complete contact information is available at: <https://pubs.acs.org/10.1021/acsnano.1c10396>

Author Contributions

[†]These authors contributed equally to this work.

Notes

The authors declare no competing financial interest.

ACKNOWLEDGMENTS

The authors are grateful for the support received from the National Key R&D Project from the Minister of Science and Technology (nos. 2016YFA0202701 and 2016YFA0202704) and the Beijing Municipal Science and Technology Commission (no. Z171100002017017).

REFERENCES

- (1) Zhao, X.; Askari, H.; Chen, J. Nanogenerators for Smart Cities in the Era of 5G and Internet of Things. *Joule* **2021**, *5*, 1391–1431.
- (2) Liu, L.; Guo, X.; Lee, C. Promoting Smart Cities into the 5G Era with Multi-Field Internet of Things (IoT) Applications Powered with Advanced Mechanical Energy Harvesters. *Nano Energy* **2021**, *88*, 106304.
- (3) Ahmed, A.; Hassan, I.; El-Kady, M. F.; Radhi, A.; Jeong, C. K.; Selvaganapathy, P. R.; Zu, J.; Ren, S.; Wang, Q.; Kaner, R. B. Integrated Triboelectric Nanogenerators in the Era of the Internet of Things. *Adv. Sci.* **2019**, *6*, 1802230.
- (4) Zhang, Q.; Li, L.; Wang, T.; Jiang, Y.; Tian, Y.; Jin, T.; Yue, T.; Lee, C. Self-Sustainable Flow-Velocity Detection via Electromagnetic/Triboelectric Hybrid Generator Aiming at IoT-Based Environment Monitoring. *Nano Energy* **2021**, *90*, 106501.
- (5) Ding, Y.; Jin, M.; Li, S.; Feng, D. Smart Logistics Based on the Internet of Things Technology: An Overview. *Int. J. Loist.: Res. Appl.* **2021**, *24*, 323–345.
- (6) Lian, Y.; Yang, Q.; Xie, W.; Zhang, L. Cyber-Physical System Based Heuristic Planning and Scheduling Method for Multiple Automatic Guided Vehicles in Logistics Systems. *IEEE Trans. Industr. Inform.* **2021**, *17*, 7882–7893.
- (7) Lee, C.; Lv, Y.; Ng, K.; Ho, W.; Choy, K. Design and Application of Internet of Things-Based Warehouse Management System for Smart Logistics. *Int. J. Prod. Res.* **2018**, *56*, 2753–2768.
- (8) de Koster, R.; Le-Duc, T.; Roodbergen, K. J. Design and Control of Warehouse Order Picking: A Literature Review. *Eur. J. Oper. Res.* **2007**, *182*, 481–501.
- (9) Ji, W.; Zhang, J.; Xu, B.; Tang, C.; Zhao, D. Grasping Mode Analysis and Adaptive Impedance Control for Apple Harvesting Robotic Grippers. *Comput. Electron. Agr.* **2021**, *186*, 106210.
- (10) Chen, F.; Selvaggio, M.; Caldwell, D. Dexterous Grasping with Manipulability Selection Using an Industrial Mobile Manipulator with Visual Guidance. *IEEE Trans. Industr. Inform.* **2019**, *15*, 1202–1210.
- (11) Alyahya, S.; Wang, Q.; Bennett, N. Application and Integration of an RFID-Enabled Warehousing Management System – A Feasibility Study. *J. Ind. Inf. Integration* **2016**, *4*, 15–25.
- (12) Majidi, C. Soft Robotics: A Perspective-Current Trends and Prospects for the Future. *Soft Robot.* **2014**, *1*, 5–11.
- (13) Yang, H.; Chen, Y.; Sun, Y.; Hao, L. A Novel Pneumatic Soft Sensor for Measuring Contact Force and Curvature of a Soft Gripper. *Sens. Actuator A Phys.* **2017**, *266*, 318–327.
- (14) El-Atab, N.; Mishra, R.; Al-Modaf, F.; Joharji, L.; Alsharif, A.; Alamoudi, H.; Diaz, M.; Qaiser, N.; Hussain, M. Soft Actuators for Soft Robotic Applications: A Review. *Adv. Intell. Syst.* **2020**, *2*, 2070102.
- (15) Fan, F.-R.; Tian, Z.-Q.; Wang, Z. L. Flexible Triboelectric Generator. *Nano Energy* **2012**, *1*, 328–334.
- (16) Zou, H.; Zhang, Y.; Guo, L.; Wang, P.; He, X.; Dai, G.; Zheng, H.; Chen, C.; Wang, A.; Xu, C.; Wang, Z. L. Quantifying the Triboelectric Series. *Nat. Commun.* **2019**, *10*, 1427.
- (17) Chen, A.; Zhang, C.; Zhu, G.; Wang, Z. L. Polymer Materials for High-Performance Triboelectric Nanogenerators. *Adv. Sci.* **2020**, *7*, 2000186.
- (18) Jin, T.; Sun, Z.; Li, L.; Zhang, Q.; Zhu, M.; Zhang, Z.; Yuan, G.; Chen, T.; Tian, Y.; Hou, X.; Lee, C. Triboelectric Nanogenerator Sensors for Soft Robotics Aiming at Digital Twin Applications. *Nat. Commun.* **2020**, *11*, 5381.
- (19) Pu, X.; Guo, H.; Tang, Q.; Chen, J.; Feng, L.; Liu, G.; Wang, X.; Xi, Y.; Hu, C. G.; Wang, Z. L. Rotation Sensing and Gesture Control of a Robot Joint via Triboelectric Quantization Sensor. *Nano Energy* **2018**, *54*, 453–460.
- (20) Qin, K.; Chen, C.; Pu, X.; Tang, Q.; He, W.; Liu, Y.; Zeng, Q.; Liu, G.; Guo, H.; Hu, C. G. Magnetic Array Assisted Triboelectric Nanogenerator Sensor for Real-Time Gesture Interaction. *Nano-Micro Lett.* **2021**, *13*, 51.
- (21) Zhang, C.; Tang, W.; Han, C. B.; Fan, F. R.; Wang, Z. L. Theoretical Comparison, Equivalent Transformation and Conjunction Operations of Electromagnetic Induction Generator and Triboelectric

Nanogenerator for Harvesting Mechanical Energy. *Adv. Mater.* **2014**, *26*, 3580–3591.

(22) Wang, Z. L. Triboelectric Nanogenerators as New Energy Technology and Self-Powered Sensors – Principles, Problems and Perspectives. *Faraday Discuss.* **2014**, *176*, 447–458.

(23) Wu, C. S.; Wang, A. C.; Ding, W. B.; Guo, H. Y.; Wang, Z. L. Triboelectric Nanogenerator: A Foundation of the Energy for the New Era. *Adv. Energy Mater.* **2019**, *9*, 1802906.

(24) Wang, J.; Li, Y.; Xie, Z.; Xu, Y.; Zhou, J.; Cheng, T. H.; Zhao, H. W.; Wang, Z. L. Cylindrical Direct-Current Triboelectric Nanogenerator with Constant Output Current. *Adv. Energy Mater.* **2020**, *10*, 1904227.

(25) Wang, Z. L. On Maxwell's Displacement Current for Energy and Sensors: The Origin of Nanogenerators. *Mater. Today* **2017**, *20*, 74–82.

(26) Wang, Z. L. Triboelectric Nanogenerator (TENG) – Sparking an Energy and Sensor Revolution. *Adv. Energy Mater.* **2020**, *10*, 2000137.

(27) Zhou, Y. S.; Zhu, G.; Niu, S. M.; Liu, Y.; Bai, P. S.; Jing, Q.; Wang, Z. L. Nanometer Resolution Self-Powered Static and Dynamic Motion Sensor Based on Micro-Grated Triboelectrification. *Adv. Mater.* **2014**, *26*, 1719–1724.

(28) Zhang, W.; Deng, L.; Yang, L.; Yang, P.; Diao, D.; Wang, P.; Wang, Z. L. Multilanguage-Handwriting Self-Powered Recognition Based on Triboelectric Nanogenerator Enabled Machine Learning. *Nano Energy* **2020**, *77*, 105174.

(29) Shuai, L.; Guo, Z.; Zhang, P.; Wan, J.; Pu, X.; Wang, Z. L. Stretchable, Self-Healing, Conductive Hydrogel Fibers for Strain Sensing and Triboelectric Energy-Harvesting Smart Textiles. *Nano Energy* **2020**, *78*, 105389.

(30) Xu, C.; Wang, A.; Zou, H.; Zhang, B.; Zhang, C.; Zi, Y.; Pan, L.; Wang, P.; Feng, P.; Lin, Z.; Wang, Z. L. Raising the Working Temperature of a Triboelectric Nanogenerator by Quenching down Electron Thermionic Emission in Contact-Electrification. *Adv. Mater.* **2018**, *30*, 1803968.

(31) Hu, Y.; Wang, X.; Li, H.; Li, H.; Li, Z. Effect of Humidity on Tribological Properties and Electrification Performance of Sliding-Mode Triboelectric Nanogenerator. *Nano Energy* **2020**, *71*, 104640.

(32) Pu, X.; Guo, H.; Chen, J.; Wang, X.; Xi, Y.; Hu, C. G.; Wang, Z. L. Eye Motion Triggered Self-Powered Mechnosensational Communication System Using Triboelectric Nanogenerator. *Sci. Adv.* **2017**, *3*, e1700694.

(33) Rus, D. L.; Tolley, M. T. Design, Fabrication and Control of Soft Robots. *Nature* **2015**, *521*, 467–475.

(34) Clark, J. A.; Cheng, J. C. Y.; Leung, K. S. Mechanical Properties of Normal Skin and Hypertrophic Scars. *Burns* **1996**, *22*, 443–446.

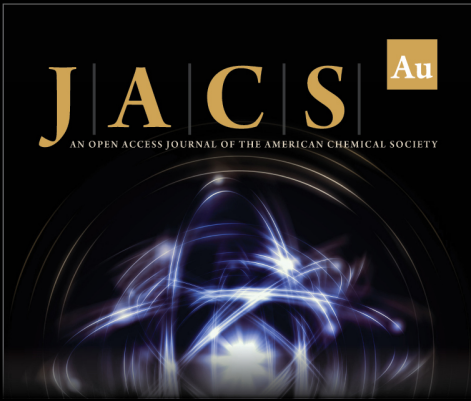
(35) Yap, H. K.; Ng, H. Y.; Yeow, C. H. High-Force Soft Printable Pneumatics for Soft Robotic Applications. *Soft Robot.* **2016**, *3*, 144.

(36) Sun, Z.; Zhu, M.; Zhang, Z.; Chen, Z.; Shi, Q.; Shan, X.; Yeow, R.; Lee, C. Artificial Intelligence of Things (AIoT) Enabled Virtual Shop Applications Using Self-Powered Sensor Enhanced Soft Robotic Manipulator. *Adv. Sci.* **2021**, *8*, 2100230.

(37) Zhu, M.; Sun, Z.; Zhang, Z.; Shi, Q.; He, T.; Liu, H.; Chen, T.; Lee, C. Haptic-Feedback Smart Glove as a Creative Human-Machine Interface (HMI) for Virtual/Augmented Reality Applications. *Sci. Adv.* **2020**, *6*, eaaz8693.

(38) Hung, C.; Zeng, S.; Lee, C.; Li, W. End-To-End Deep Learning by MCU Implementation: An Intelligent Gripper for Shape Identification. *Sensors* **2021**, *21*, 891.

(39) Liu, H.; Deng, Y.; Guo, D.; Fang, B.; Sun, F.; Yang, W. An Interactive Perception Method for Warehouse Automation in Smart Cities. *IEEE Trans. Industr. Inform.* **2021**, *17*, 830–838.



JACS Au
AN OPEN ACCESS JOURNAL OF THE AMERICAN CHEMICAL SOCIETY

Editor-in-Chief
Prof. Christopher W. Jones
Georgia Institute of Technology, USA

Open for Submissions 

pubs.acs.org/jacsau  ACS Publications
Most Trusted. Most Cited. Most Read.